Electronic Supplementary Information (ESI)

Effect of surface acidity of cyano-bridged polynuclear metal complexes on catalytic activity for hydrolysis of organophosphates

*Hiroyasu Tabe, Chihiro Terashima and Yusuke Yamada**,

Department of Applied Chemistry and Bioengineering, Graduate School of Engineering, Osaka City University, Osaka 558-8585, Japan.

* To whom correspondence should be addressed.
E-mail: ymd@a-chem.eng.osaka-cu.ac.jp.

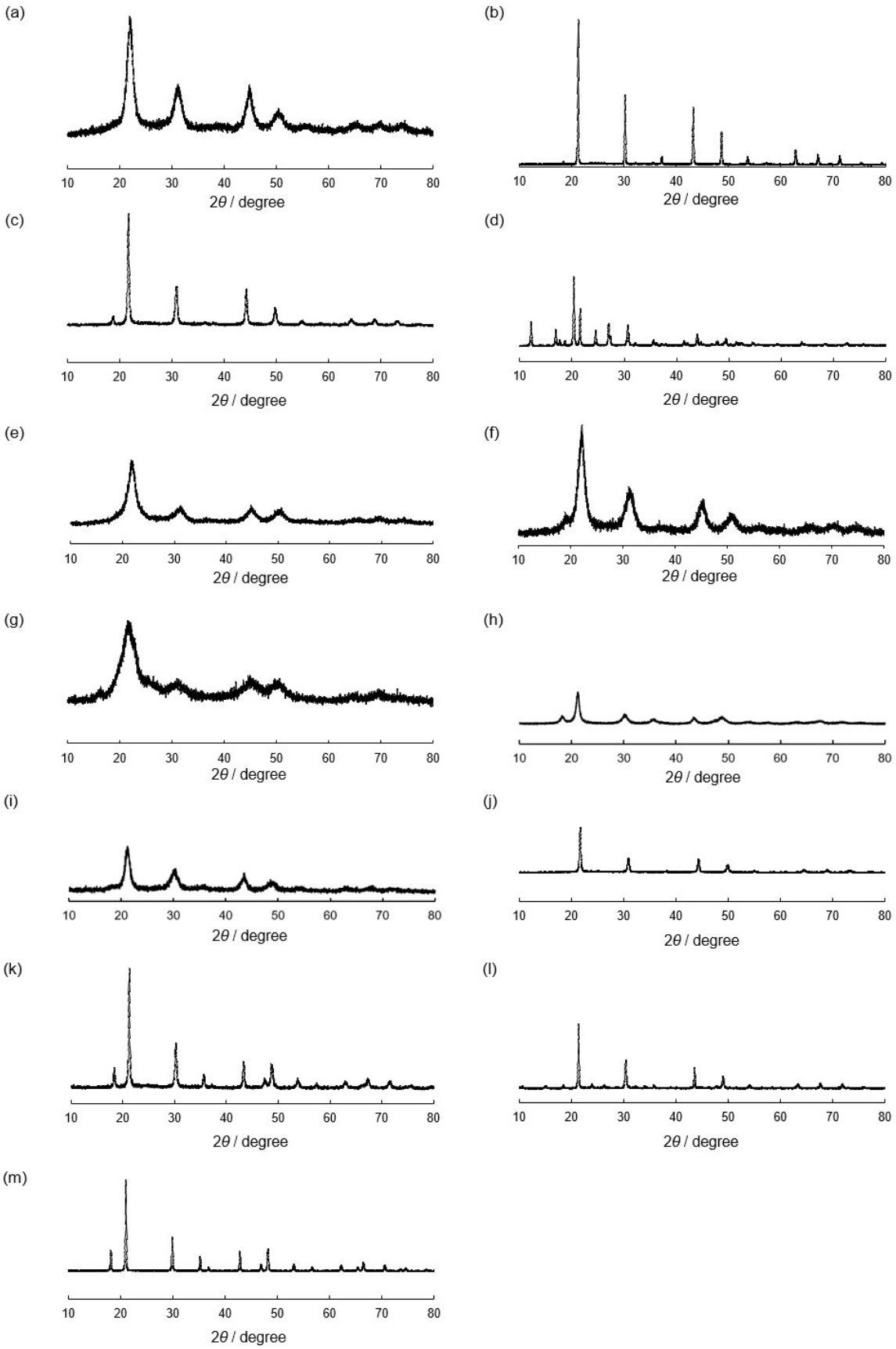

Fig. S1 Powder X-ray diffraction patterns of cyano-bridged polynuclear metal complexes. [(a) $[Fe^{III}(H_2O)_{1.5}]_{4/3}[Fe^{II}(CN)_6]$, (b) $[Mn^{II}(H_2O)_2]_{1.5}[Fe^{III}(CN)_6]$, (c) $[Co^{II}(H_2O)_2]_{1.5}[Fe^{III}(CN)_6]$, (d) $[Zn^{II}(H_2O)_2]_{1.5}[Fe^{III}(CN)_6]$, (e) $Ga^{III}[Fe^{III}(CN)_6]$, (f) $[Ga^{III}(H_2O)_{1.5}]_{4/3}[Fe^{II}(CN)_6]$, (g) $Fe^{III}[Co^{III}(CN)_6]$, (h) $Fe^{III}[Ir^{III}(CN)_6]$, (i) $[Fe^{III}(H_2O)_{1.5}]_{4/3}[Ru^{II}(CN)_6]$, (j) $[Fe^{II}(H_2O)_2]_{1.5}[Co^{III}(CN)_6]$, (k) $[Fe^{II}(H_2O)_2]_{1.5}[Ir^{III}(CN)_6]$, (l) $[Fe^{II}(H_2O)_3]_2[Ru^{II}(CN)_6]$ and (m) $Fe^{II}[Pt^{IV}(CN)_6]$]

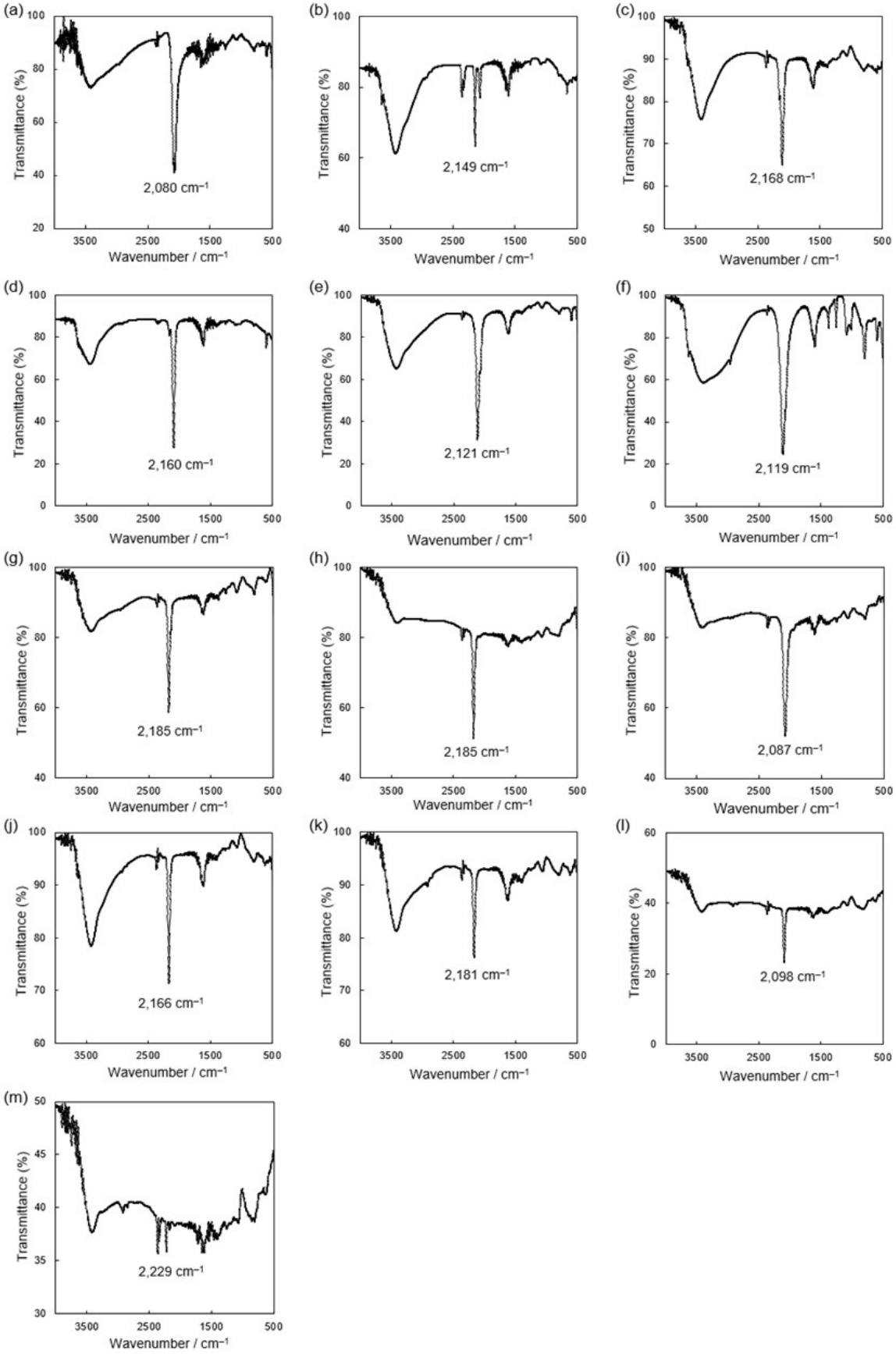

Fig. S2 IR spectra of cyano-bridged polynuclear metal complexes. [(a) $[Fe^{III}(H_2O)_{1.5}]_{4/3}[Fe^{II}(CN)_6]$, (b) $[Mn^{II}(H_2O)_2]_{1.5}[Fe^{III}(CN)_6]$, (c) $[Co^{II}(H_2O)_2]_{1.5}[Fe^{III}(CN)_6]$, (d) $[Zn^{II}(H_2O)_2]_{1.5}[Fe^{III}(CN)_6]$, (e) $Ga^{III}[Fe^{III}(CN)_6]$, (f) $[Ga^{III}(H_2O)_{1.5}]_{4/3}[Fe^{II}(CN)_6]$ (g) $Fe^{III}[Co^{III}(CN)_6]$, (h) $Fe^{III}[Ir^{III}(CN)_6]$, (i) $[Fe^{III}(H_2O)_{1.5}]_{4/3}[Ru^{II}(CN)_6]$, (j) $[Fe^{II}(H_2O)_2]_{1.5}[Co^{III}(CN)_6]$, (k) $[Fe^{II}(H_2O)_2]_{1.5}[Ir^{III}(CN)_6]$, (l) $[Fe^{II}(H_2O)_3]_2[Ru^{II}(CN)_6]$ and (m) $Fe^{II}[Pt^{IV}(CN)_6]$]

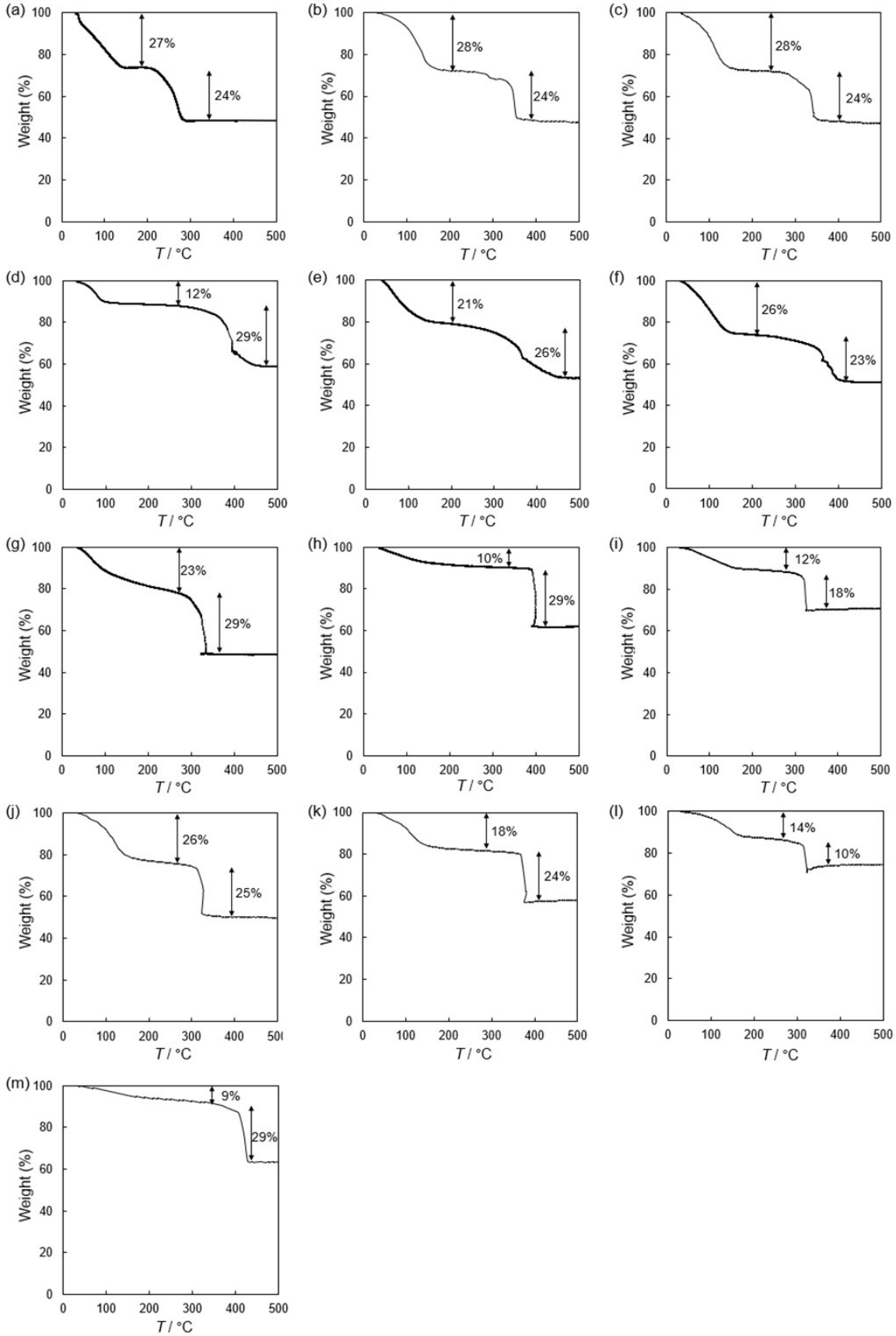

Fig. S3 Thermogravimetric analyses of cyano-bridged polynuclear metal complexes in an air flow. [(a) $[Fe^{III}(H_2O)_{1.5}]_{4/3}[Fe^{II}(CN)_6]$, (b) $[Mn^{II}(H_2O)_2]_{1.5}[Fe^{III}(CN)_6]$, (c) $[Co^{II}(H_2O)_2]_{1.5}[Fe^{III}(CN)_6]$, (d) $[Zn^{II}(H_2O)_2]_{1.5}[Fe^{III}(CN)_6]$, (e) $Ga^{III}[Fe^{III}(CN)_6]$, (f) $[Ga^{III}(H_2O)_{1.5}]_{4/3}[Fe^{II}(CN)_6]$ (g) $Fe^{III}[Co^{III}(CN)_6]$, (h) $Fe^{III}[Ir^{III}(CN)_6]$, (i) $[Fe^{III}(H_2O)_{1.5}]_{4/3}[Ru^{II}(CN)_6]$, (j) $[Fe^{II}(H_2O)_2]_{1.5}[Co^{III}(CN)_6]$, (k) $[Fe^{II}(H_2O)_2]_{1.5}[Ir^{III}(CN)_6]$, (l) $[Fe^{II}(H_2O)_3]_2[Ru^{II}(CN)_6]$ and (m) $Fe^{II}[Pt^{IV}(CN)_6]$]

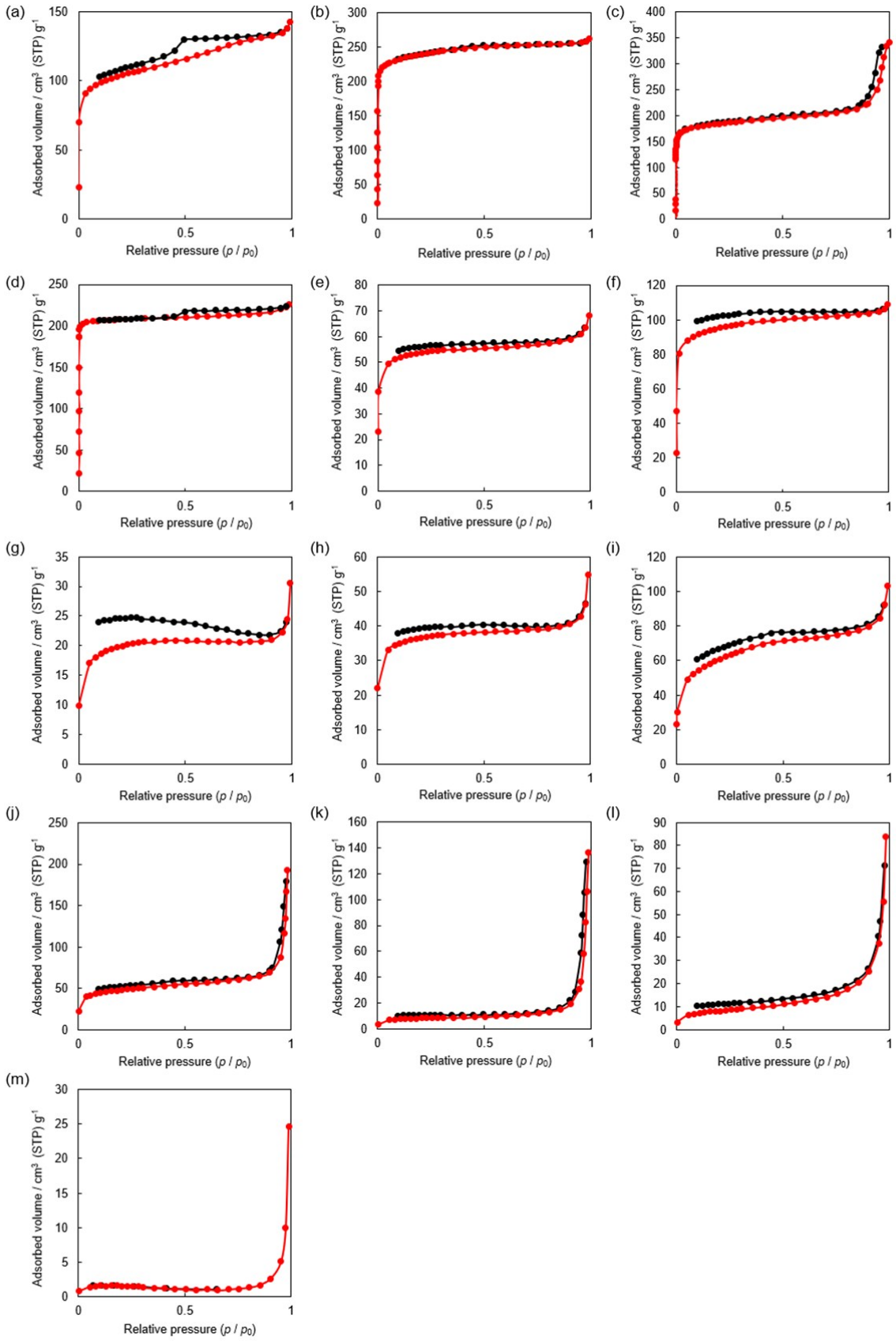

Fig. S4 Nitrogen adsorption (red)–desorption (black) isotherms at –196 °C for cyano-bridged polynuclear metal complexes. [(a) $[Fe^{III}(H_2O)_{1.5}]_{4/3}[Fe^{II}(CN)_6]$, (b) $[Mn^{II}(H_2O)_2]_{1.5}[Fe^{III}(CN)_6]$, (c) $[Co^{II}(H_2O)_2]_{1.5}[Fe^{III}(CN)_6]$, (d) $[Zn^{II}(H_2O)_2]_{1.5}[Fe^{III}(CN)_6]$, (e) $Ga^{III}[Fe^{III}(CN)_6]$, (f) $[Ga^{III}(H_2O)_{1.5}]_{4/3}[Fe^{II}(CN)_6]$, (g) $Fe^{III}[Co^{III}(CN)_6]$, (h) $Fe^{III}[Ir^{III}(CN)_6]$, (i) $[Fe^{III}(H_2O)_{1.5}]_{4/3}[Ru^{II}(CN)_6]$, (j) $[Fe^{II}(H_2O)_2]_{1.5}[Co^{III}(CN)_6]$, (k) $[Fe^{II}(H_2O)_2]_{1.5}[Ir^{III}(CN)_6]$, (l) $[Fe^{II}(H_2O)_3]_2[Ru^{II}(CN)_6]$ and (m) $Fe^{II}[Pt^{IV}(CN)_6]$]

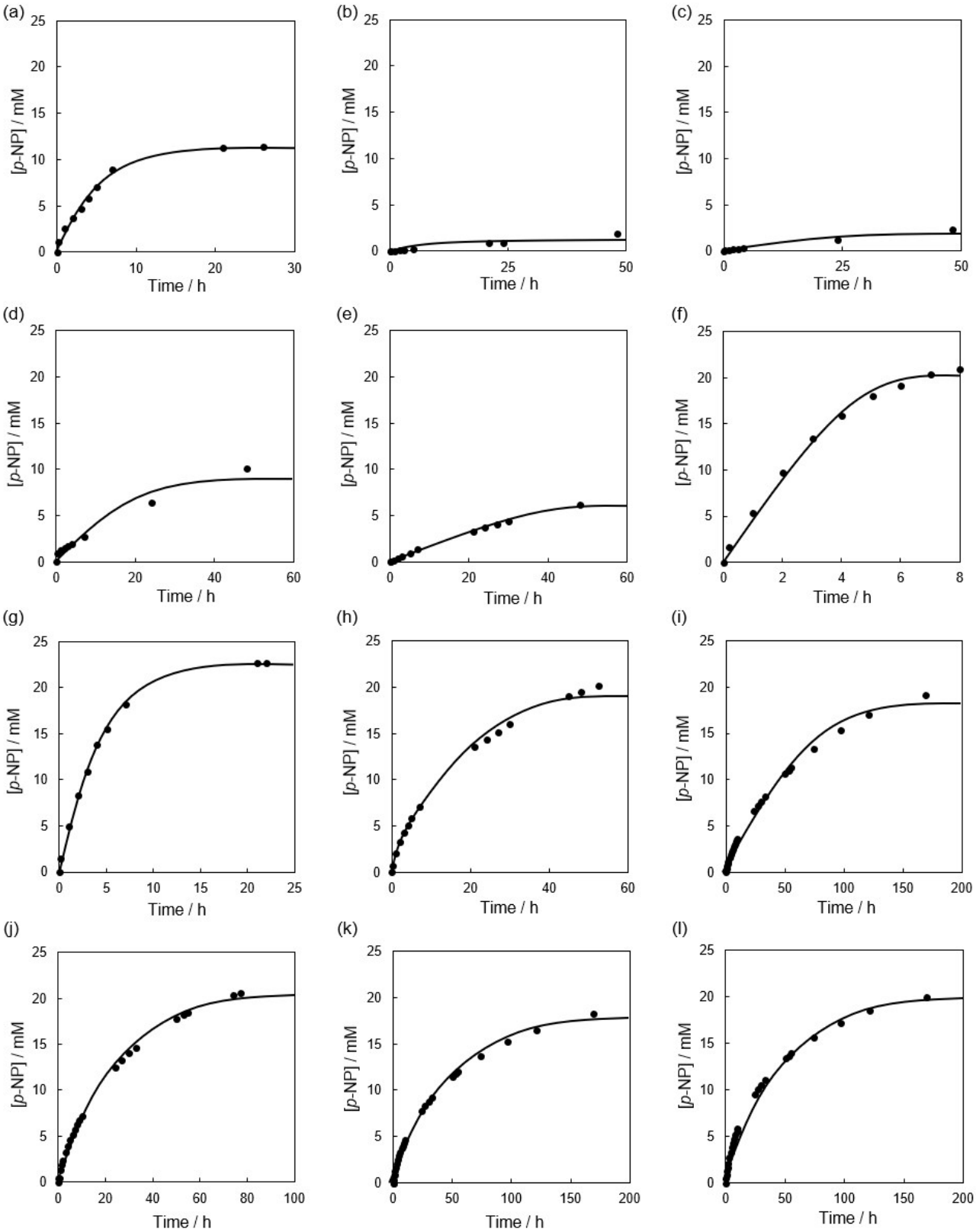

Fig. S5 Time profiles of *p*-nitrophenol (*p*-NP) formation by hydrolysis of *p*-nitrophenyl phosphate (*p*-NPP, 25 mM) in a HEPES buffer (100 mM, pH 8.3, 0.75 mL) containing cyano-bridged polynuclear metal complexes. [(a) $[Mn^{II}(H_2O)_2]_{1.5}[Fe^{III}(CN)_6]$, (b) $[Co^{II}(H_2O)_2]_{1.5}[Fe^{III}(CN)_6]$, (c) $[Zn^{II}(H_2O)_2]_{1.5}[Fe^{III}(CN)_6]$, (d) $Ga^{III}[Fe^{III}(CN)_6]$, (e) $[Ga^{III}(H_2O)_{1.5}]_{4/3}[Fe^{II}(CN)_6]$, (f) $Fe^{III}[Co^{III}(CN)_6]$, (g) $Fe^{III}[Ir^{III}(CN)_6]$, (h) $[Fe^{III}(H_2O)_{1.5}]_{4/3}[Ru^{II}(CN)_6]$, (i) $[Fe^{II}(H_2O)_2]_{1.5}[Co^{III}(CN)_6]$, (j) $[Fe^{II}(H_2O)_2]_{1.5}[Ir^{III}(CN)_6]$, (k) $[Fe^{II}(H_2O)_3]_2[Ru^{II}(CN)_6]$ and (l) $Fe^{II}[Pt^{IV}(CN)_6]$]

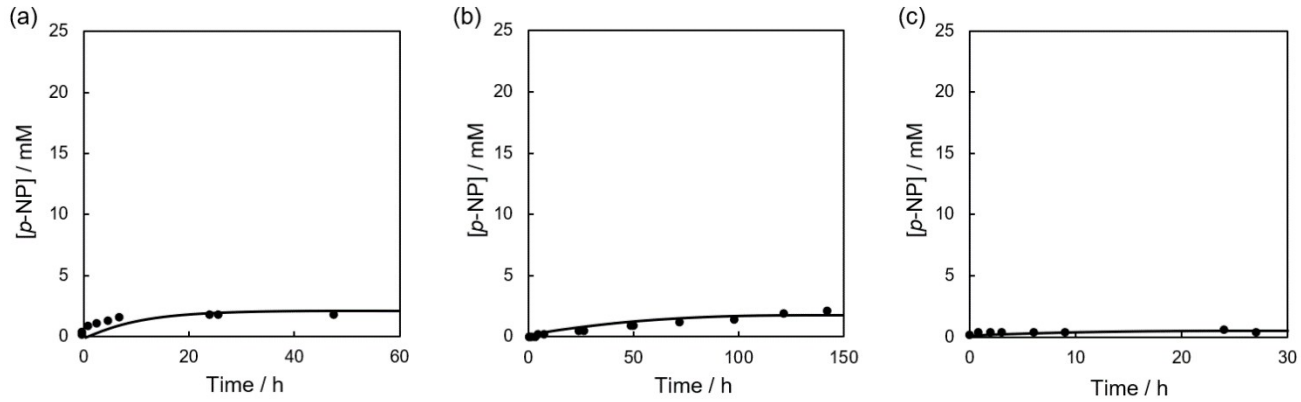

Fig. S6 Time profiles of *p*-nitrophenol (*p*-NP) formation by hydrolysis of paraoxon methyl (PO, 25 mM) in a HEPES buffer (100 mM, pH 8.3, 0.75 mL) containing cyano-bridged polynuclear metal complexes. [(a) $[Fe^{III}(H_2O)_{1.5}]_{4/3}[Fe^{II}(CN)_6]$, (b) $Fe^{III}[Co^{III}(CN)_6]$ and (c) in the absence of catalysts]

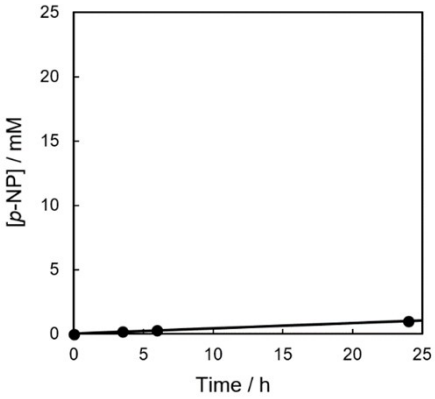

Fig. S7 Time profiles of *p*-nitrophenol (*p*-NP) formation by hydrolysis of *p*-nitrophenyl phosphate (*p*-NPP, 25 mM) in a HEPES buffer (100 mM, pH 8.3, 0.75 mL) containing $Fe(NO_3)_3$ ([*p*-NPP]/[Fe] = 100).

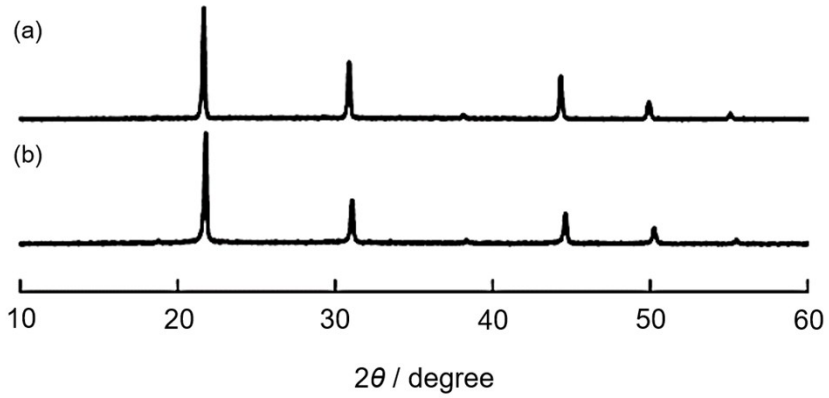

Fig. S8 Powder X-ray diffraction patterns of $[Fe^{III}(H_2O)_{1.5}]_{4/3}[Fe^{II}(CN)_6]$ (Prussian blue) nanoparticles in (a) cubic shape (PB-cube) and (b) spherical shape (PB-sphere).

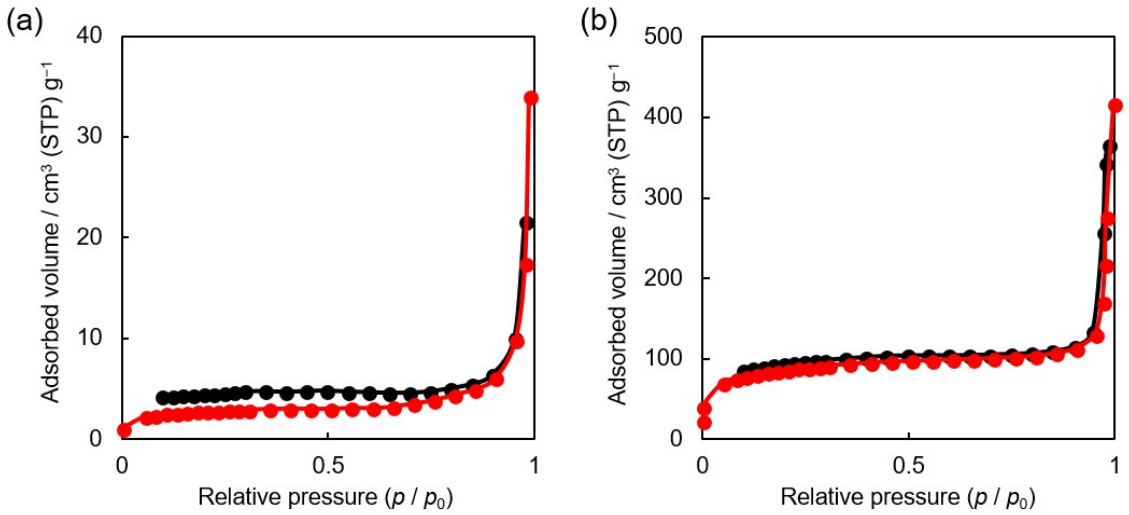

Fig. S9 Nitrogen adsorption (red)–desorption (black) isotherms at −196 °C for $[Fe^{III}(H_2O)_{1.5}]_{4/3}[Fe^{II}(CN)_6]$ (Prussian blue) nanoparticles in (a) cubic shape (PB-cube) and (b) spherical shape (PB-sphere).

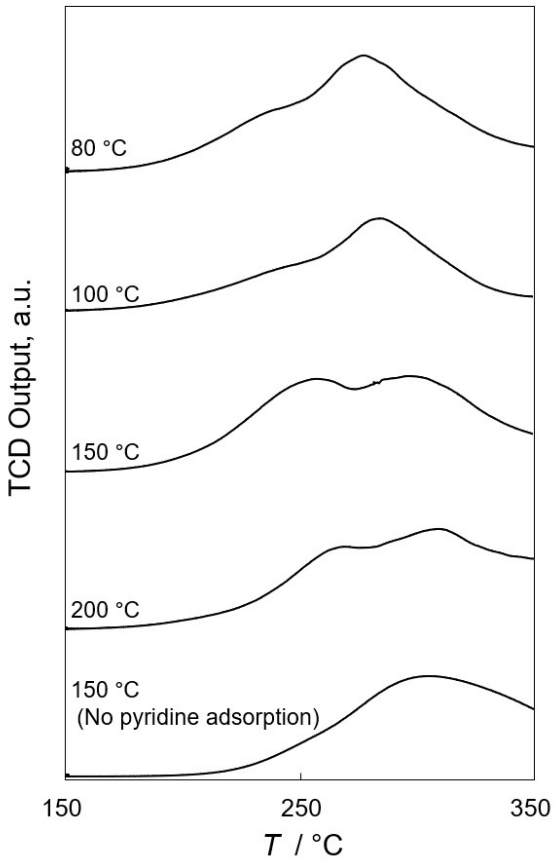

Fig. S10 Temperature-programmed desorption (TPD) spectra of $[Fe^{III}(H_2O)_{1.5}]_{4/3}[Fe^{II}(CN)_6]$ (58.9 mg, the ramp rate of 10 °C min^{-1}) after pretreatment for removal of physisorbed water for 1 h at temperatures of 80, 100, 150 and 200 °C, adsorption of pyridine (5 kPa, 100 °C for 30 min) and removal of excess pyridine (150 °C, 30 min) with a flow of helium (He, 30 mL min^{-1}). The TPD spectrum without pyridine adsorption was obtained after pretreatment at 150 °C.

Comments: A sharp TPD peak at around 264 °C after pretreatment at 150 °C was assigned to pyridine desorption, because this peak was indistinct for $[Fe^{III}(H_2O)_{1.5}]_{4/3}[Fe^{II}(CN)_6]$ without pyridine adsorption. The second peak at around 300 °C was assigned to loss of CN ligands of $[Fe^{III}(H_2O)_{1.5}]_{4/3}[Fe^{II}(CN)_6]$ as confirmed by the TPD spectrum of $[Fe^{III}(H_2O)_{1.5}]_{4/3}[Fe^{II}(CN)_6]$ without pyridine adsorption. The TPD peak at around 264 °C was not clearly observed for $[Fe^{III}(H_2O)_{1.5}]_{4/3}[Fe^{II}(CN)_6]$ pretreated at 80, 100 and 200 °C. Thus, the appropriate pretreatment temperature is 150 °C.

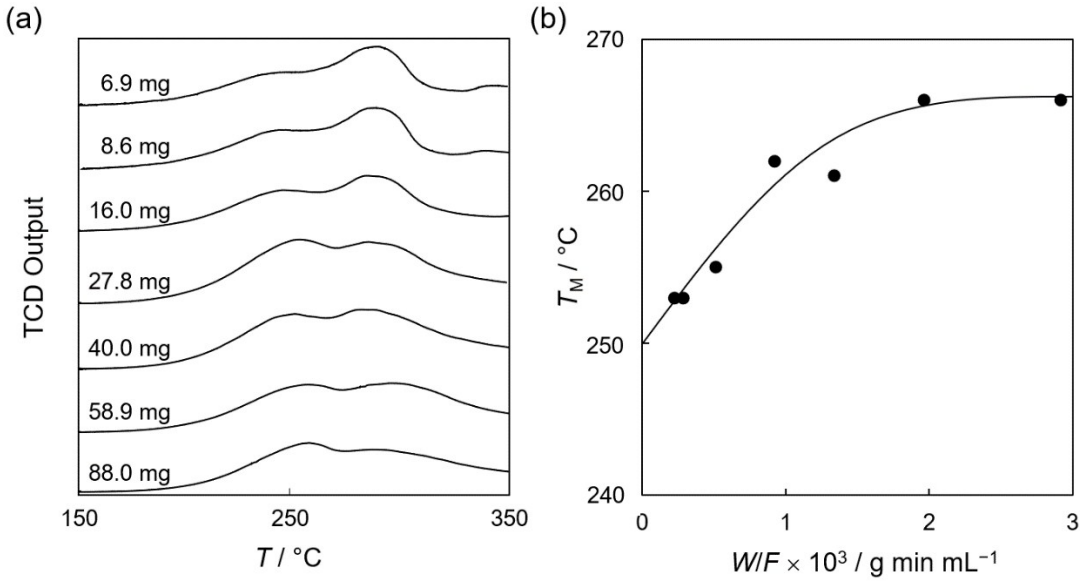

Fig. S11 (a) Temperature-programmed desorption (TPD) spectra of various weight of $[Fe^{III}(H_2O)_{1.5}]_{4/3}[Fe^{II}(CN)_6]$ (the ramp rate of 10 °C min^{-1}) after pretreatment for removal of physisorbed water (150 °C, 1 h), adsorption of pyridine (5 kPa, 100 °C for 30 min) and removal of excess pyridine (150 °C, 30 min) with a flow of helium (He, 30 mL min^{-1}). (b) Relation of temperature of pyridine-desorption maximum (T_M) to W/F where W and F represent weight of samples and a flow rate of He, respectively.

Comments: The weight of $[Fe^{III}(H_2O)_{1.5}]_{4/3}[Fe^{II}(CN)_6]$ used for the TPD measurements (W) was optimized, because the temperature of pyridine-desorption maximum (T_M) depends on W/F, where F is the flow rate of He. Constant T_M can be obtained when W is large enough, because readsorption of the desorbed pyridine occurs. Eq.11 can

$$\ln \frac{T_M^2}{\beta} = \frac{\Delta H}{RT_M} + \ln\left[\frac{(1-\theta)^2 V_S \Delta H}{FAR}\right] \quad (11)$$

be derived under consideration of the balance of pyridine with desorption and readsoprtion, where β, ΔH, R, F, θ, V_s and A stand for ramp rate, heat of desorption of pyridine, the gas constant, gas flow rate, coverage of catalyst surface, catalyst volume and pre-exponential factor, respectively.[S1] TPD measurements carried out with changing W (6.9–88.0 mg) showed the shift of T_M from 251 to 264 °C (Figure S10a). The plot of T_M vs. W/F suggests that T_M is almost constant when W/F is larger than 2.0×10^3 (Figure S10b). Thus, the used weight of samples was larger than 60 mg with the flow rate of He of 30 mL min^{-1} for further analyses.

Reference

S1 M. Nakano, T. Hironaka, S. Fujii and K. Sekizawa, *Toyo Soda Kenkyu Hokoku*, 1985, **29**, 3−11.

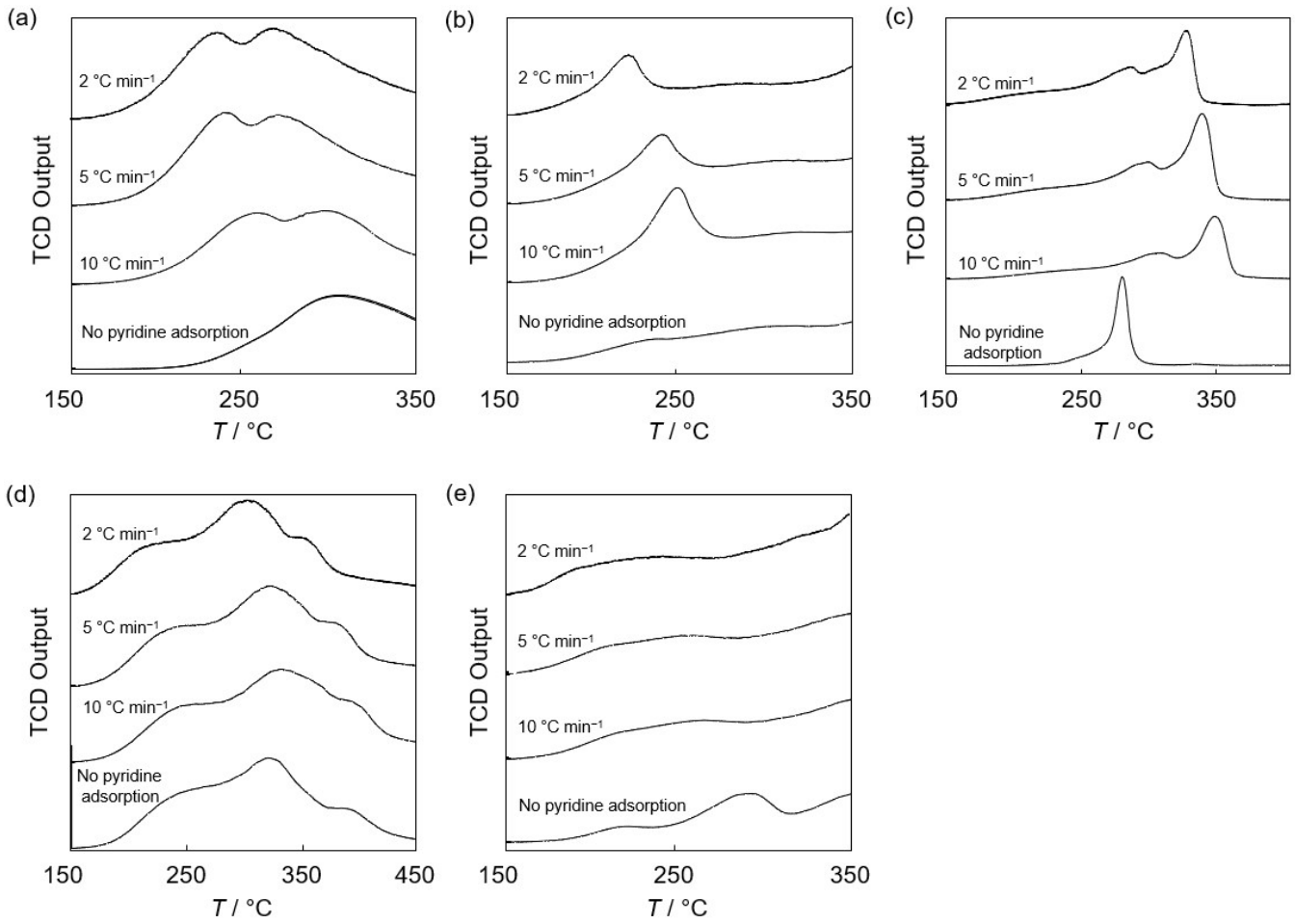

Fig. S12 Temperature-programmed desorption (TPD) of pyridine from (a) $[Fe^{III}(H_2O)_{1.5}]_{4/3}[Fe^{II}(CN)_6]$, (b) $Fe^{III}[Co^{III}(CN)_6]$, (c) $[Mn^{II}(H_2O)_2]_{1.5}[Fe^{III}(CN)_6]$, (d) $Ga^{III}[Fe^{III}(CN)_6]$ and (e) $[Fe^{II}(H_2O)_2]_{1.5}[Co^{III}(CN)_6]$. TPD measurements were performed by heating with various ramp rates ranging from 2 to 10 °C min^{-1} after pretreatment at 150 °C, 1 h, adsorption of pyridine (5 kPa, 100 °C for 30 min) and removal of excess pyridine (150 °C, 30 min) with a flow of helium (30 mL min^{-1}). The TPD spectra without pyridine adsorption was obtained after pretreatment at 150 °C.

Comments: Multiple peaks appeared for (d) $Ga^{III}[Fe^{III}(CN)_6]$ and (e) $[Fe^{II}(H_2O)_2]_{1.5}[Co^{III}(CN)_6]$ without pyridine adsorption. These peaks can be assigned to loss of chemisorbed water molecules and CN ligands, which were also confirmed by TGA (Fig. S3).

Table S1 Weight and molar ratios of iron (Fe), potassium (K) and another metal species (M) in each cyano-bridged polynuclear metal complex determined by X-ray fluorescence measurements

Complex	M	Weight ratio M/Fe	Molar ratio M/Fe	Weight ratio K/Fe	Molar ratio K/Fe
$[Fe^{III}(H_2O)_{1.5}]_{4/3}[Fe^{II}(CN)_6]$	–	–	–	0.04	0.1
$Fe^{III}[Co^{III}(CN)_6]$	Co	0.9	0.9	0	0
$Fe^{III}[Ir^{III}(CN)_6]$	Ir	3.8	1.1	0	0
$[Fe^{III}(H_2O)_{1.5}]_{4/3}[Ru^{II}(CN)_6]$	Ru	1.9	0.8	0.05	0.1
$[Fe^{II}(H_2O)_2]_{1.5}[Co^{III}(CN)_6]$	Co	0.7	0.6	0.02	0.1
$[Fe^{II}(H_2O)_2]_{1.5}[Ir^{III}(CN)_6]$	Ir	2.1	1.4	0.04	0
$[Fe^{II}(H_2O)_3]_2[Ru^{II}(CN)_6]$	Ru	1.0	1.8	0.04	0.1
$Fe^{II}[Pt^{IV}(CN)_6]$	Pt	3.3	1.4	0	0
$[Mn^{II}(H_2O)_2]_{1.5}[Fe^{III}(CN)_6]$	Mn	1.5	1.5	0.03	0
$[Co^{II}(H_2O)_2]_{1.5}[Fe^{III}(CN)_6]$	Co	1.5	1.4	0.05	0.1
$[Zn^{II}(H_2O)_2]_{1.5}[Fe^{III}(CN)_6]$	Zn	2.4	2.1	0.05	0.1
$Ga^{III}[Fe^{III}(CN)_6]$	Ga	1.2	0.9	0	0
$[Ga^{III}(H_2O)_{1.5}]_{4/3}[Fe^{II}(CN)_6]$	Ga	1.6	1.3	0	0

Table S2 Lattice parameters (*a*), CN stretching frequencies (ν_{CN}), Brunauer−Emmett−Teller (BET) surface areas (*S*), external surface areas obtained by *t*-Plot (S_{ext}), pore diameters obtained by the Barrett−Joyner−Halenda (BJH) method and the microporous (MP) method and average particle sizes of $[Fe^{III}(H_2O)_{1.5}]_{4/3}[Fe^{II}(CN)_6]$ (Prussian blue) prepared by a conventional method (PB), Prussian blue in cubic shape (PB-cube) and Prussian blue in spherical shape (PB-sphere)

Complex	*a* / Å	ν_{CN} / cm^{-1}	*S* / $m^2\ g^{-1}$	S_{ext} / $m^2\ g^{-1}$	Pore diameter / nm	Average particle size / nm
PB	10.2	2080	384	9	3.5	–
PB-cube	10.3	2080	10	3	0.6	300
PB-sphere	10.2	2086	300	25	0.6	150

Table S3 Summary of temperature of pyridine-desorption maximum (T_M), heat of pyridine desorption (ΔH) of cyano-bridged polynuclear metal complexes, and initial rate for catalytic hydrolysis of *p*-nitrophenyl phosphate (*p*-NPP) using the complexes

Complex	T_M / °C[a]	ΔH / kJ mol^{-1}	v_0 / mol L^{-1} h^{-1} [b]
$[Fe^{III}(H_2O)_{1.5}]_{4/3}[Fe^{II}(CN)_6]$	264	152	3.1×10^{-3}
$Fe^{III}[Co^{III}(CN)_6]$	254	160	5.3×10^{-3}
$[Mn^{II}(H_2O)_2]_{1.5}[Fe^{III}(CN)_6]$	309	222	6.5×10^{-3}
$Ga^{III}[Fe^{III}(CN)_6]$	402	176	6.1×10^{-3}
$[Fe^{II}(H_2O)_2]_{1.5}[Co^{III}(CN)_6]$	243	98	1.0×10^{-3}

[a]Temperature of pyridine-desorption maximum from each complex with a ramp rate of 10 °C min^{-1}. Each complex was preadsorbed pyridine after pretreatment in a He flow (30 mL min^{-1}) at 150°C. [b]Initial rates were determined based on the *p*-NPP conversions for 10 min.